Principles of Space Plasma Wave Instrument Design

Donald A. Gurnett

Department of Physics and Astronomy, The University of Iowa, Iowa City, Iowa

Space plasma waves span the frequency range from somewhat below the ion cyclotron frequency to well above the electron cyclotron frequency and plasma frequency. Because of the large frequency range involved, the design of space plasma wave instrumentation presents many interesting challenges. This chapter discusses the principles of space plasma wave instrument design. The topics covered include: performance requirements, electric antennas, magnetic antennas, and signal processing. Where appropriate, comments are made on the likely direction of future developments.

INTRODUCTION

In this chapter we discuss the principles of space plasma wave instrument design. The study of space plasma waves has its origins in early ground-based studies of very-low-frequency (VLF) radio signals. The earliest record of a VLF radio signal of natural origin is by *Preece* [1894], who describes a number of unusual audio frequency signals that he detected while studying the propagation characteristics of a long-distance transmission line. Some years later, *Barkhausen* [1919] using a rudimentary vacuum-tube amplifier identified a class of whistling VLF signals now known as whistlers. Progress on the understanding of these radio signals was slow. After several years of investigation, *Eckersley* [1935] correctly postulated that whistlers were produced by lightning. However, the propagation path and mechanism that dispersed the signal into a long whistling tone was unknown. It was not until the early 1950s that *Storey* [1953] was able to provide a satisfactory explanation of whistlers. He showed that the dispersion occurred as the signal propagated along the Earth's magnetic field in a plasma mode of propagation now known as the whistler mode.

In addition to whistlers, a number of other signals were discovered during the early ground-based era of VLF research that were clearly not produced by lightning. Among the best known of these are "dawn chorus" [*Storey*, 1953; *Allcock*, 1957] and "auroral hiss" [*Burton and Boardman*, 1933; *Duncan and Ellis*, 1959; *Dowden*, 1959]. These signals eventually came to be known as VLF emissions, since they were believed to be emitted by charged particles in the ionized upper levels of the Earth's atmosphere [*Ellis*, 1957; *Gallet*, 1959]. However, the exact emission mechanism remained largely unknown. For a review of early ground-based observations of whistlers and VLF emissions, see *Helliwell* [1965].

With the launch of the first Earth-orbiting satellites in the late 1950s, radio receivers were soon being carried into orbit to investigate the origin of VLF emissions. The first satellites with receivers specifically designed to study VLF emissions were Alouette 1 (launched Sept. 29, 1962) and Injun 3 (launched Dec. 13, 1962). Alouette 1 carried an electric dipole antenna [*Barrington and Belrose*, 1963], and Injun 3 carried a magnetic loop antenna [*Gurnett and O'Brien*, 1964]. These and other similar instruments soon showed that a wide variety of complex wave phenomena existed in the Earth's magnetosphere, which is a region of magnetized plasma surrounding the Earth. These included not only whistler-mode emissions, but also a variety of new

Measurement Techniques in Space Plasmas: Fields
Geophysical Monograph 103

modes of propagation that had never previously been observed. These waves are now known as space plasma waves. For a review of space plasma waves, see *Shawhan* [1979].

It is now known that plasma waves play a fundamental role in the physics of space plasmas. Virtually all space plasma investigations now include a plasma wave instrument. The purpose of this paper is to discuss the basic principles of plasma wave instrument design. The presentation is organized into four topics. Section II discusses performance requirements, Section III describes electric antennas, Section IV describes magnetic antennas, and Section V describes on-board signal processing.

PERFORMANCE REQUIREMENTS

Before going into a detailed discussion of the design of a plasma wave instrument, it is useful to first discuss the basic performance requirements. Three types of requirements are discussed: (1) the number of field components measured, (2) the frequency range, and (3) the sensitivity and dynamic range.

Number of Field Components Measured

As is well known, two types of waves can propagate in a plasma: electromagnetic and electrostatic [*Stix*, 1962]. Electromagnetic waves have both an electric field and a magnetic field, and electrostatic waves have only an electric field. Since these two types of waves interact quite differently with the plasma, it is important to be able to distinguish electromagnetic waves from electrostatic waves. The best way to do this is to use both an electric antenna and a magnetic antenna. If the wave is detected on both types of antennas, then it is an electromagnetic wave. If the wave is detected only with the electric antenna then it is an electrostatic wave. Thus, the first basic design requirement is to include both electric and magnetic antennas.

Next, one must next decide on the number of components to be measured. Of course, full three-axis measurements are ideal. The main reason for including three axis measurements is to determine the direction of the propagation vector, $\vec{k}$. For electromagnetic waves, magnetic field measurements provide the best method of determining the $\vec{k}$ vector direction. Maxwell's equation, $\vec{\nabla}\cdot\vec{B} = 0$, guarantees that $\vec{k}$ is perpendicular to plane of rotation of the magnetic field. Except at high frequencies (i.e., in the free space regime), there is no comparable relationship for the electric field. To determine the propagation direction of electrostatic waves, three axis electric field measurements are required. If mass or other restrictions prohibit three-axis measurements, the next best alternative is single-axis measurements. The $\vec{k}$ direction cannot be obtained from two-axis measurements.

Frequency Range

An important consideration in the design of any plasma wave instrument is the frequency range. The frequency range of interest extends from somewhat below the ion cyclotron frequency to somewhat above either the electron plasma frequency or the electron cyclotron frequency, whichever is larger. The electron plasma frequency is given by $f_{pe} = 9\sqrt{n}$ kHz, where n is the electron density in cm^{-3}, the electron cyclotron frequency is given by $f_{ce} = 28$ B Hz, where B is the magnetic field strength in nT, and the ion cyclotron frequency is given by $f_{ci} = (m_e/m_i)f_{ce}$, where m_e/m_i is the electron-to-ion mass ratio. In space plasmas, the ion cyclotron frequency is often quite small. For example, in the outer regions of the Earth's magnetosphere, the proton cyclotron frequency is only about 0.1 Hz. In the Earth's magnetosphere, the highest frequency of interest is usually the electron plasma frequency, which extends up to about 5 to 10 MHz in the ionosphere. At Jupiter, where the magnetic field is much stronger, the electron cyclotron frequency can be as high as 40 MHz, well above the electron plasma frequency. As can be seen from the above examples, the frequency range of potential interest for plasma wave measurements is enormous, extending from approximately 0.1 Hz to 10 MHz at Earth, and from approximately 0.01 Hz to 40 MHz at Jupiter. One of the most difficult challenges of modern plasma wave instrument design is to provide satisfactory measurements over such a large frequency range.

When considering the frequency range to be investigated, it is often useful to make a distinction between local and remote measurements. If the spacecraft spends most of its time far from the planet, as is often the case for planetary flybys and eccentric orbiting spacecraft, the local electron cyclotron frequency and plasma frequency are usually much smaller than the corresponding values near the planet. Under these circumstances the lower part of the frequency range is dominated by locally generated plasma waves, and the upper part of the frequency range (above the local electron plasma frequency and cyclotron frequency) is dominated by remotely generated radio emissions. Both parts of the spectrum are important, but require somewhat different techniques. For locally generated plasma waves, both electric and magnetic fields must be measured in order to distinguish electromagnetic waves from electrostatic waves. On the other hand, for remotely

generated radio emissions there is little point to measuring both the electric and the magnetic fields, since the waves are known to be electromagnetic. Thus, at frequencies above the local electron plasma frequency and cyclotron frequency, it is usually adequate to measure either the electric field or the magnetic field, but not both.

Sensitivity and Dynamic Range

To be successful, a plasma wave instrument must be able to detect waves over a very large range of intensities. Locally generated plasma waves, such as in planetary bow shocks and in auroral acceleration regions, are often extremely intense. At the opposite extreme, various types of thermally excited waves are extremely weak and difficult to detect. Although weak, some of these waves have proven to be extremely valuable for plasma diagnostics (see, for example, *Meyer-Vernet* [1979], and *Meyer-Vernet et al.* [1997]). To give a rough indication of the dynamic range that must be accommodated, Figures 1 and 2 show representative electric and magnetic field spectrums for various plasma wave phenomena observed in the Earth's magnetosphere. As one can see, the dynamic range requirements are very severe, typically 100 to 120 dB.

ELECTRIC ANTENNAS

Two types of electric antennas have been used for wave electric field measurements: monopoles and dipoles. A monopole responds to the potential difference between a single antenna element and a ground plane, usually the spacecraft body, whereas a dipole antenna responds to the potential difference between two antenna elements extending outward in opposite direction. The term "monopole," as used above, is actually a misnomer, since the spacecraft body effectively acts as the second element of a dipole. Although monopole antennas have been used on a number of spacecraft [*Scarf et al.*, 1965; *Warwick et al.*, 1977], this type of antenna is very susceptible to spacecraft-generated electrical interference, so dipoles are almost always used for modern plasma wave instruments.

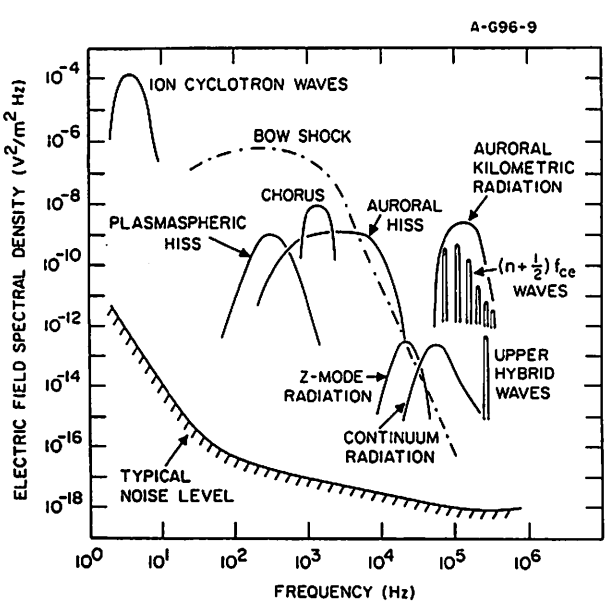

Figure 1. Representative electric field spectrums for various plasma wave phenomena observed in the Earth's magnetosphere.

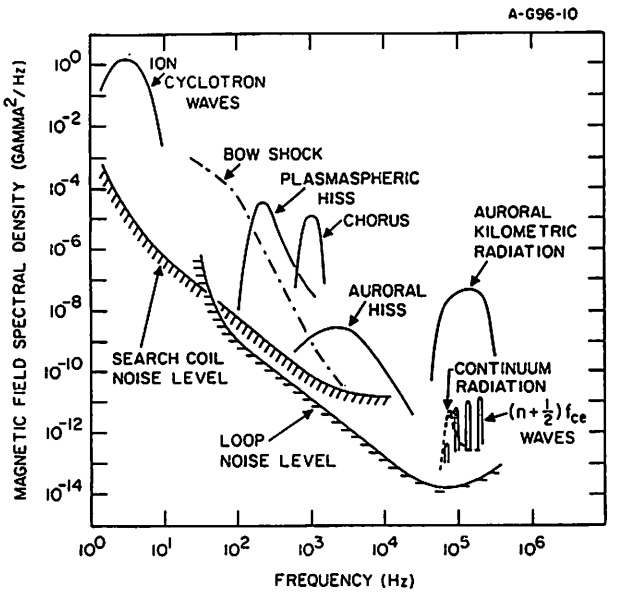

Figure 2. Representative magnetic field spectrums for various plasma wave phenomena observed in the Earth's magnetosphere.

Over the years, two types of electric dipole antennas have evolved: (1) cylindrical dipoles, and (2) spherical double probes. They differ mainly in the geometry of the sensing elements. For a cylindrical dipole, the elements consist of two conducting cylinders extending outward in opposite directions from the spacecraft body, as in the top panel of Figure 3. The radius of the elements, a, is normally much smaller than the tip-to-tip length, L. Typical dimensions are a = 0.1 to 1 cm and L = 100 m. A differential amplifier in the spacecraft body provides a signal, ΔV, that is proportional to the potential difference between the elements. For a spherical double probe, the two elements consist of conducting spheres mounted on the end of booms, as in the bottom panel of Figure 3. The center-to-center separation, L, between the spheres is normally much larger than the radius, r, of the spheres. Typical dimensions are r = 10 cm and L = 100 m.

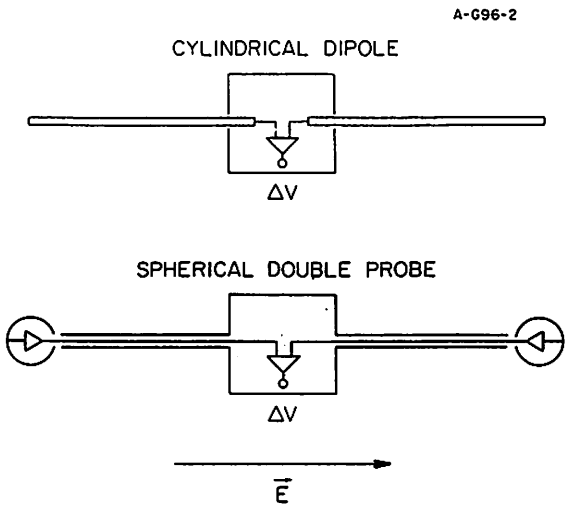

Figure 3. The geometry of a cylindrical electric dipole antenna and a spherical double probe. A differential amplifier in the spacecraft body provides a voltage output, ΔV, that is proportional to the voltage difference between the elements.

Preamplifiers are usually located in the spheres to provide low impedance signals to a differential amplifier in the spacecraft body.

For most types of waves detected in space plasmas, it is usually the case that the wavelengths are much longer than the length of the antenna ($\lambda \gg L$). The response of an electric dipole antenna is then characterized by a quantity called the effective length. The effective length is defined by

$$L_{eff} = \frac{\Delta V}{E} \quad , \qquad (1)$$

where E is the electric field component along the axis of the antenna and ΔV is the open circuit potential difference between the elements (i.e., the voltage difference that would exist in the absence of any electrical load). The effect of an electrical load is usually represented by an equivalent circuit of the type shown in Figure 4. The voltage generator, $\Delta V_{in} = E\, L_{eff}$, represents the voltage inducted by the electric field, Z_A represents the antenna impedance, and Z_L represents the load impedance imposed by the spacecraft at the base of the antenna. The effective length and antenna impedance depend on a number of factors, including (1) the geometry of the antenna, (2) the frequency and wavelength of the incident wave, and (3) the parameters of the plasma. A quantitative analysis is only possible in certain limiting cases, as discussed below.

High Frequency Limit

If the wave frequency is well above the electron plasma frequency and cyclotron frequency, the effects of the plasma are essentially negligible. The antenna then responds as if it were in free space. In free space the response of an electric dipole antenna is usually analyzed by using the reciprocity theorem [*Jordan*, 1950], which states that the coupling between a transmitter and a receiver is unaffected by interchanging the receiver and the transmitter. Thus, instead of analyzing the receiving properties of the antenna, one can just as well analyze the radiation properties of the antenna.

For a cylindrical dipole that is short compared to the wavelength, it is well known that the radiation properties can be represented by charges, ±Q, that are uniformly distributed along the two antenna elements [*Jordan*, 1950]. Since the centers of the two charge distributions are located at the centers of the elements, it is obvious that the equivalent dipole moment is obtained by separating the charges by a distance of L/2. The effective length is then $L_{eff} = L/2$. For a spherical double probe the analysis is even simpler. Since the charges on the two elements are separated by a distance L, it immediately follows that the effective length is $L_{eff} = L$.

Since the fields around an electrically short ($\lambda \ll L$) dipole are almost purely electrostatic, the antenna impedance is almost purely capacitive and can be represented by a capacitive reactance, $Z_A = 1/(i\omega C_A)$, where C_A is the capacitance of the element relative to free space. For a cylindrical dipole, the antenna capacitance is given to a good approximation by

$$C_A = \frac{2\pi\epsilon_0(L/2)}{[\ell n(L/2a) - 1]} \quad , \qquad (2)$$

where a is the radius of the element and ε_0 is the permittivity of free space [*Jordan*, 1950]. For a spherical

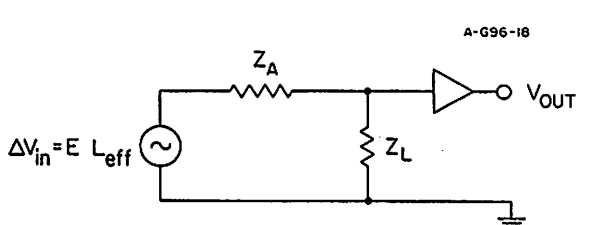

Figure 4. The equivalent circuit of an electric antenna. ΔV_{in} is the voltage induced by the applied electric field, Z_A is the antenna impedance and Z_L is the load impedance at the base of the antenna.

double probe, the antenna capacitance is given to a good approximation by

$$C_A = 4\pi\epsilon_0 r \quad . \tag{3}$$

where r is the radius of the sphere.

To provide maximum power transfer from the source to the load, it is well known that the load impedance must be the complex conjugate of the source impedance, $Z_L = Z_A^*$. This relationship is known as the maximum power transfer theorem [*Jordan*, 1950]. Since the impedance of a short ($L \ll \lambda$) electric dipole antenna is almost purely capacitive, maximum power transfer is achieved when the load impedance is almost purely inductive, with $Z_L = -1/(i\omega C_A)$. In practice it is extremely difficult to achieve this impedance matching condition. Instead, the usual procedure is to maximize the voltage delivered to the preamplifier. This condition is achieved by making the load impedance large compared to the antenna impedance, $Z_L > Z_A$. At high frequencies the load impedance can usually be represented by a capacitive reactance, $Z_L = 1/(i\omega C_L)$. The capacitance C_L includes: (1) the capacitance from the antenna element to the spacecraft structure, (2) the capacitance of the cable that connects the antenna element to the preamplifier, and (3) the input capacitance of the preamplifier. When the load impedance is purely capacitive, one can see from the equivalent circuit in Figure 4 that the ratio of the output voltage to the input voltage is given by a simple capacitive divider

$$\frac{V_{out}}{E\, L_{eff}} = \frac{C_A}{C_A + C_L} \quad . \tag{4}$$

Maximum voltage transfer is achieved by making C_A much larger than C_L. This condition ($C_A > C_L$) is called the ideal voltmeter condition. As one can see from Equations 2 and 3, the antenna capacitance is proportional to the size of the sensing elements. Since the length, L/2, of a cylindrical dipole element is much larger than the radius, r, of a spherical double probe, the capacitance of a cylindrical dipole is much larger than the capacitance of a spherical double probe. Thus, it is usually much easier to achieve ideal voltmeter operation for a cylindrical dipole than for a spherical double probe.

Low Frequency Limit

If the wave frequency is comparable or less than the electron plasma frequency and cyclotron frequency, then the effects of the plasma can no longer be ignored. When an object is placed in a plasma, it is well known that a plasma sheath forms around the object. If the object is exposed to ultraviolet light, which is usually the case in space, then two types of sheaths can occur: (1) a positive ion sheath, and (2) a photoelectron sheath. A positive ion sheath occurs when the electron current from the plasma exceeds the emitted photoelectron current. Under these conditions the surface charges to a negative potential, thereby repelling some of the electrons and leaving the sheath with a positive charge (hence the term, positive ion sheath). Since ion currents are usually negligible, equilibrium occurs when the electron current reaching the surface is equal to the emitted photoelectron current. A positive ion sheath has a characteristic thickness that is given by the Debye length, $\lambda_D = 6.9\ (T/n)^{1/2}$ cm, where T is the electron temperature in °K, and n is the electron density in cm^{-3}. The Debye length ranges from about 1 cm in the ionosphere to about 10 m in the solar wind.

If the plasma density is so low that the electron current from the plasma cannot compensate for the emitted photoelectron current, then the surface charges to a positive potential. The positive potential inhibits the escape of photoelectrons, thereby forming a negatively charged sheath of photoelectrons around the object. This type of sheath is called a photoelectron sheath. The thickness of a photoelectron sheath depends on the intensity and spectrum of the photoelectrons and is almost completely independent of the plasma parameters. For the typical photoelectron spectrum emitted from a metal surface at 1 A.U. (astronomical unit), the shielding thickness is about 30 cm. For the plasma temperatures that are normally encountered in the Earth's magnetosphere, the transition from a positive ion sheath to a photoelectron sheath usually occurs as the electron density drops below about 10^2 to 10^3 cm^{-3}.

A full treatment of the response of an electric antenna to a wave in a magnetized plasma is quite complicated and is well beyond the scope of this review. A relatively simple model that seems to work well under a wide range of plasma parameters was introduced by *Storey* [1965]. Also, see *Fahleson* [1967] and *Kelley et al.* [1970]. This model assumes that the wave can be described locally by an electrostatic potential, and that the potential is linearly coupled to the antenna through the sheath that surrounds the antenna. If the thickness of the sheath is small compared to the tip-to-tip length of the antenna (i.e., $\lambda_D \ll L$), then the sheath forms a layer of nearly constant thickness around the antenna. The approximate geometries of the sheaths that form around the antenna are then as shown in Figures 5 and 6. To analyze the response of the antenna, Storey assumed that the potential in the plasma is

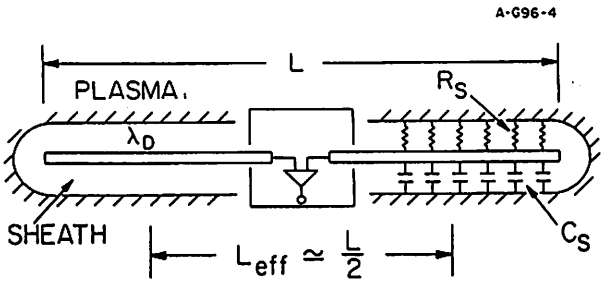

Figure 5. The geometry of the plasma sheath that forms around a cylindrical electric dipole antenna. The thickness of the sheath is given by the Debye length, λ_D. Potentials in the plasma are coupled to the antenna via the sheath resistance, R_S, and the sheath capacity, C_S. The effective length, L_{eff}, of a cylindrical dipole is one-half the tip-to-tip length, L.

coupled to the antenna via a sheath resistance R_S and a sheath capacitance C_S that are uniformly distributed over the surface of the antenna (see the right-hand sides of Figures 5 and 6).

Since ion currents are usually negligible, the primary contribution to the sheath resistance comes from the electrons. If we restrict the analysis to frequencies well below the electron plasma frequency and cyclotron frequency, the sheath resistance can be computed from Langmuir probe theory. Langmuir probe theory deals with the equilibrium voltage-current (V-I) characteristic of an object immersed in a plasma [*Langmuir*, 1929]. It is well known that the V-I curve for a positive ion sheath has the form shown in Figure 7. For small amplitude signals, the resistance of the sheath is determined by the differential slope, $R_S = \partial V/\partial I$, evaluated at some bias point I_{Bias}. For a Maxwellian plasma, it is easy to show that the resistance of a positive ion sheath is given by

$$R_S = \frac{U_e}{I_p + I_i + I_{Bias}} \quad . \tag{5}$$

where $U_e = \kappa T_e/e$ is the electron temperature expressed in Volts, I_p is the emitted photoelectron current, and I_i is the

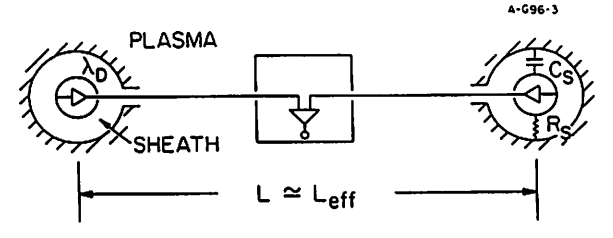

Figure 6. The geometry of the plasma sheath that forms around a spherical double probe. The effective length, L_{eff}, of a spherical double probe is the center-to-center distance between the spheres.

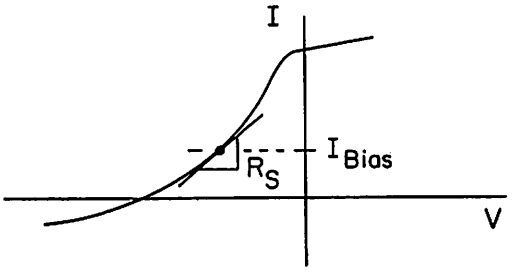

Figure 7. The voltage-current, V-I, characteristics of a conducting object placed in a plasma. The sheath resistance, R_S, is the slope of the V-I curve evaluated at a bias current, I_{Bias}.

incident ion current. For a photoelectron sheath, the sheath resistance is given by

$$R_S = \frac{U_p}{I_e - I_i - I_{Bias}} \quad , \tag{6}$$

where $U_p \simeq 1.5$ Volts is the characteristic energy of the photoelectron spectrum (see *Cauffman and Gurnett* [1972]).

To compute the sheath capacity, C_S, it is usually assumed that the sheath consists of a capacitor, with the antenna element acting as one conductor and the plasma acting as the other conductor. Since electrons are essentially excluded from a positive ion sheath, the interior of the capacitor is assumed to be free space. A similar assumption is used for a photosheath. Ignoring end effects, the capacitance of a cylindrical dipole is then given by

$$C_S = 2\pi\epsilon_0(L/2)/\ell n(\lambda_D/a) \quad , \tag{7}$$

where λ_D is the thickness of the sheath and a is the radius of the element. The above formula assumes that $a \ll \lambda_D$, a condition that is almost always satisfied. For a spherical double probe, the capacitance is given by

$$C_S = 4\pi\epsilon_0 r\left(1 + \frac{r}{\lambda_D}\right) \quad , \tag{8}$$

where λ_D is the thickness of the sheath and r is the radius of the sphere.

Having described the essential characteristics of the sheath that forms around an antenna, we next address the question of the effective length. If an electric field E_0 is applied along the axis of the antenna, then the potential in the plasma is given by $\Phi = -E_0 z$, where z is the distance along the axis of the antenna. If the R-C coupling is uniform along the axis of the antenna, it is easy to see that

the potential of an element is simply the average of the potential along the axis of that element, i.e., $V = -E_0(L/4)$. The voltage difference between the two elements is then given by $\Delta V = -E_0(L/2)$, so the effective length is $L_{eff} = L/2$. Since a spherical double probe responds to the potentials at $z = -L/2$ and $z = L/2$, it is easy to see that the voltage difference between the elements is given by $\Delta V = -E_0 L$, so the effective length is $L_{eff} = L$. It is interesting to note that in the low frequency plasma limit, the effective lengths are exactly the same as in the high frequency-free space limit.

Based on the above discussion, it follows that the response of an electric dipole antenna can be represented by the equivalent circuit shown in Figure 8. The antenna impedance Z_A is determined by the sheath resistance R_S and the sheath capacitance C_S, and the load impedance Z_L is determined by the load capacitance C_L and the load resistance R_L. The ratio of the output voltage to the input voltage is then given by a simple impedance division

$$\frac{\Delta V_{out}}{E\, L_{eff}} = \frac{Z_L}{Z_A + Z_L} \quad . \tag{9}$$

Since we want the electric field measurement to be as independent of the plasma parameters as possible it is clear that the antenna should be operated as an ideal voltmeter (i.e., $Z_L \gg Z_A$, so that $\Delta V_{out} = E\, L_{eff}$). At high frequencies the impedance ratio is mainly controlled by the capacitances and is given by

$$\frac{\Delta V_{out}}{E\, L_{eff}} = \frac{C_S}{C_S + C_L} \quad . \tag{10}$$

This is the same result that was obtained in the free space limit, except the antenna capacitance is now replaced by the sheath capacitance. At low frequencies the impedance ratio is mainly controlled by the resistances and is given by

$$\frac{\Delta V_{out}}{E\, L_{eff}} = \frac{R_L}{R_S + R_L} \quad . \tag{11}$$

To operate as an ideal voltmeter, the sheath capacitance must be much greater than the load capacitance ($C_S \gg C_L$), and the sheath resistance must be much less than the load resistance, i.e., ($R_S \ll R_L$). The transition between the capacitive and resistive regimes is controlled by the sheath capacity and sheath resistance. If the $C_S \gg C_L$ and $R_S \ll R_L$, it is easy to show that this transition occurs at a R-C transition frequency given by $\omega_{RC} = 1/R_S C_S$. Resistive coupling dominates for $\omega < \omega_{RC}$ and capacitive coupling dominates for $\omega > \omega_{RC}$.

Unfortunately, it is not always easy to achieve the conditions required to operate the antenna as an ideal voltmeter (i.e., $C_S \gg C_L$ and $R_S \ll R_L$). Because of its much larger capacitance, a cylindrical dipole again has a significant advantage over a spherical double probe. For example, if $\lambda_D = 1$ m, L = 100 m, a = 1 cm, and r = 10 cm, then the capacitance of a cylindrical dipole is about 1000 pf, whereas the capacitance of a spherical double probe is only about 10 pf. Thus, in the capacitive coupling regime it is much easier to achieve ideal voltmeter operation for a cylindrical dipole than for a spherical double probe. A cylindrical dipole also has another advantage that is related to the relative variability of the sheath resistance and the sheath capacity. Of these two parameters, the sheath resistance is much more variable than the sheath capacitance. This can be seen by comparing Equations 5 and 6 for the sheath resistance with Equations 7 and 8 for the sheath capacity. The sheath resistance is strongly controlled by the electron temperature, U_e, and the electron current, I_e, both of which vary over large ranges. In contrast, the antenna capacitance is controlled by the logarithmic term in Equation 7 and by the $(1 + r/\lambda_D)$ term in Equation 8, neither of which depend strongly on the plasma parameters (usually $r \ll \lambda_D$). Since we want the sheath coupling to be as independent of the plasma parameters as possible, it is clear from the above discussion that the antenna should be operated in the capacitive regime over as large a frequency range as possible. This means that the RC transition frequency, $\omega_{RC} = 1/R_S C_S$, should be made as low as possible, which implies that the capacitance should be as large as possible. Since a cylindrical dipole has a much larger capacitance than a spherical double probe, a cylindrical dipole can be operated in the capacitive regime over a substantially larger frequency range than a spherical double probe.

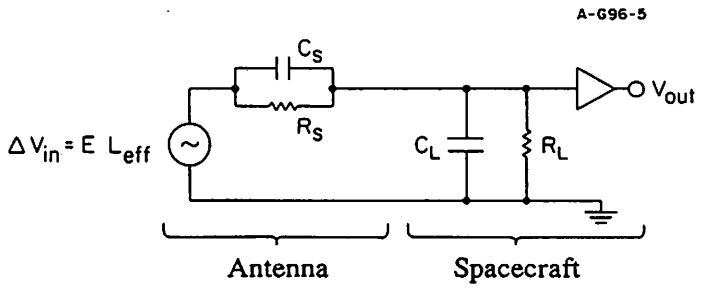

Figure 8. The equivalent circuit of an antenna immersed in a plasma. The resistance and capacitance of the sheath are represented by R_S and C_S, and the resistance and capacitance of the load are represented by R_L and C_L.

Although ideal voltmeter operation can usually be achieved in the capacitive coupling regime ($\omega > \omega_{RC}$), at low plasma densities it is extremely difficult to achieve ideal voltmeter operation in the resistive coupling regime ($\omega < \omega_{RC}$). In the presence of solar ultraviolet radiation, the sheath is always a photoelectron sheath at low plasma densities (i.e., when $I_p + I_i + I_{bias} > I_e$). For this type of sheath the antenna resistance is inversely proportional to the incident electron current (see Equation 6). Since the incident electron current varies in direct proportion to the electron density, as the electron density decreases the antenna resistance increases, eventually reaching the point where the ideal voltmeter condition, $R_S \ll R_L$, is violated. For typical cylindrical dipole dimensions (L = 100 m and a = 0.1 cm) and a preamplifier resistance of $R_L \sim 10^9$ to 10^{10} ohm, the ideal voltmeter condition is usually violated at electron densities below about 1 to 10 cm^{-3}. The RC transition frequency at this density is typically a few tens of Hz. For a spherical double probe (r = 10 cm), the RC transition frequency under similar conditions is typically several kHz. Thus, in a low density plasma a cylindrical dipole provides sheath independent (i.e., capacitively coupled) measurements over a substantially greater frequency range than is possible with a spherical double probe. To improve the operation of a spherical double probe at low plasma densities, a bias current is often used (see *Mozer* [1969]). As shown by Equation 6, the sheath resistance can be decreased by applying an external bias current I_{Bias}. The bias current must be negative, which means that a current is drawn from the plasma. This current bias technique is commonly used for static electric field measurements, where measurements must be made down to essentially zero frequency.

Short Wavelength Effects

Electrostatic waves can sometimes have very short wavelengths. The theoretical minimum wavelength is given by $\lambda = 2\pi/\lambda_D$. If the wavelength is comparable or shorter than the length of the antenna, then the response deviates considerably from the long wavelength limit discussed in the previous section. The approach to analyzing the short wavelength response is basically the same as in the previous section, except the potential in the plasma is given by $\Phi = -(E_0/k) \sin(kz)$ instead of $\Phi = -E_0 z$. For a cylindrical dipole, the voltage difference between the elements is determined by integrating the plasma potential over the length of the antenna while taking into account the R-C coupling through the sheath. As before, end effects are ignored. Using this simple model, *Fuselier and Gurnett* [1984] have shown that in the ideal voltmeter limit, $Z_A \ll Z_L$, the response of a cylindrical dipole is given by

$$\frac{\Delta V_{out}}{E_0 L_{eff}} = \frac{\sin^2 x}{x^2} \quad , \tag{12}$$

where $x = k L_{eff}/2$ is the normalized wave number and $L_{eff} = L/2$. For a spherical double probe, the analysis is even simpler, since the spheres can be regarded as two point probes. The corresponding result for a spherical double probe is given by

$$\frac{\Delta V_{out}}{E_0 L_{eff}} = \frac{\sin x}{x} \quad , \tag{13}$$

where in this case $L_{eff} = L$.

Plots of the antenna response, $\Delta V/(E_0 L_{eff})$ as a function of the normalized wave number are shown in Figure 9 for a cylindrical dipole and a spherical double probe. In both cases the response has a transition at x = 1. For $x \ll 1$, the response asymptotically approaches the long wavelength response. For x > 1 the response decreases rapidly with increasing wavenumber, varying as $1/k^2$ for a cylindrical dipole and as 1/k for a spherical double probe, with nulls at $x = n\pi$ where n = 1, 2, 3, ···. These nulls can cause

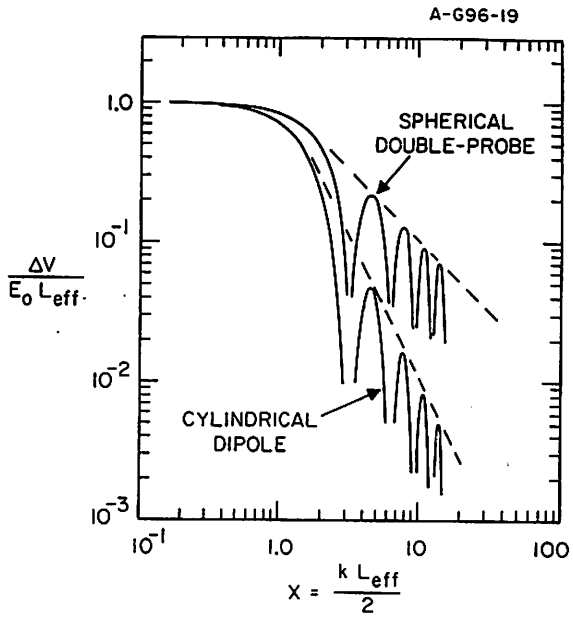

Figure 9. The response of a spherical double probe and a cylindrical dipole to wavelengths comparable or shorter than the antenna length. The parameter x is the normalized wave number ($x = kL_{eff}/2$), and L_{eff} is the effective length at long wavelengths.

interference patterns in the electric field spectrum [*Temerin*, 1979; *Fuselier and Gurnett*, 1984; *Feng et al.*, 1993]. The interference patterns are particularly noticeable on a spinning spacecraft. As the spacecraft rotates destructive interference occurs whenever the projection of the effective antenna length onto the wave vector corresponds to an integral number of wavelengths, $L_{eff} \cos \phi = n\lambda$. The geometry that leads to a null is illustrated in Figure 10. The shape and spacing of the nulls can be used to give information on the wavelength and mode of propagation of the wave. Since the response of a spherical double probe decreases less rapidly with increasing wavenumber than for a cylindrical dipole, interference effects are usually more clearly defined for a spherical double probe. It is also sometimes advantageous to measure the fractional density fluctuations, $\delta n/n$, at each probe, rather than the electric field. For a review of the techniques used to measure wavelengths in space plasmas, see *LaBelle and Kintner* [1989].

Noise Levels

Two types of noise affect the performance of an electric antenna: preamplifier noise and plasma noise. Since the impedance of an electric antenna tends to be rather large, current noise is often the most important type of noise generated by the preamplifier. This noise flows from the preamplifier into the antenna and has two components: a low-frequency component that varies as 1/f, and a high-frequency component that is nearly independent of frequency. The spectral density, $I_p^2/\Delta f$, of the current noise is determined by the type of input transistor. Usually FET transistors provide the lowest noise, although other types of transistors can be used depending on the detailed design of the preamplifier. For a typical FET preamplifier, the noise current in the high frequency range has a spectral density in the range from about 10^{-26} to 10^{-30} amp^2/Hz. The transition to the 1/f spectrum usually takes place at a frequency of about 10 to 100 Hz.

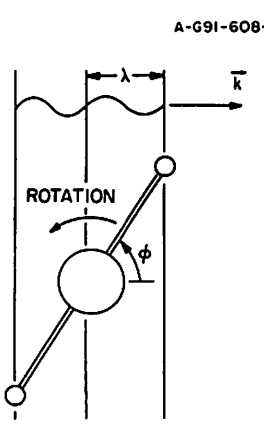

Figure 10. A sketch showing the null patterns produced by a rotating antenna when the wavelength is small compared to the length of the antenna. Nulls are produced when the projection of the effective length onto the $\vec{k}$-vector direction, $L_{eff} \cos \phi$, corresponds to an integral number of wavelengths, $n\lambda$.

There are two types of noise generated by the plasma. The first is thermal (Nyquist) noise generated by the sheath resistance R_S, and the second is shot noise caused by charged particle impacts on the antenna. The thermal noise can be represented by a current source with a spectral density $I_R^2/\Delta f = 4\kappa T_S/R_S$ in parallel with the sheath resistance R_S, where κ is Boltzmann's constant, and T_S is the sheath temperature [*Hancock*, 1961]. For a positive ion sheath the appropriate temperature for the sheath is the plasma electron temperature, since the V-I characteristic of the antenna is mainly determined by the plasma electrons. For a photoelectron sheath the appropriate temperature is the photoelectron temperature (~18,000°K). Since the electron flux is usually much higher than the ion flux, shot noise is mainly due to electron impacts. It is easy to show that the current spectral density due to electron impacts is given by $I_e^2/\Delta f = e^2\nu_e$, where e is the electronic charge and ν_e is the impact rate [*Hancock*, 1961].

If the antenna is operated as an ideal voltmeter (i.e., $Z_A \ll Z_L$), then all of the above noise currents flow through the sheath. The differential voltage spectral density between the two elements due to these noise currents is then given by

$$\frac{(\Delta V)^2}{\Delta f} = 2|Z_A|^2 \left(\frac{I_p^2}{\Delta f} + \frac{4\kappa Ts}{R_S} + e^2\nu_e \right) \quad . \qquad (14)$$

The factor of two in the above equation occurs because the noise powers from the two elements must be added when computing $(\Delta V)^2$. Using the antenna impedance model described earlier, the electric field noise level then becomes

$$\frac{E_N^2}{\Delta f} = \frac{2}{L_{eff}^2} \frac{R_S^2}{1 + \omega^2 R_S^2 C_S^2} \left(\frac{I_p^2}{\Delta f} + \frac{4\kappa Ts}{R_S} + e^2\nu_e \right) \quad . \qquad (15)$$

From the above equation one can see that the primary factors affecting the electric field noise level are the effective length L_{eff}, the sheath resistance R_S, the sheath capacitance C_S, and the electron impact rate ν_e. Clearly the effective length should be made as large as possible, subject only to the constraint that the antenna should not be longer than the wavelength ($L < \lambda$). To analyze the remaining factors, the resistive and capacitive coupling

regimes must be considered separately. In the resistive coupling regime, $\omega R_S C_S \ll 1$, the noise level is minimized by making R_S and ν_e as small as possible. However, this leads to opposing requirements. Both R_S and ν_e depend on the collecting area of the antenna. From Equations 5 and 6 one can see that R_S is minimized by increasing the area of the antenna (i.e., by making I_p and I_e as large as possible). On the other hand, increasing the area of the antenna increases the impact rate, hence the shot noise. Usually the emphasis is on maintaining ideal voltmeter operation (i.e., maximizing the area in order to minimize R_S) even though this increases the shot noise. In the capacitive coupling region, $\omega R_S C_S \gg 1$, the noise level is minimized by making R_S and C_S as large as possible, and ν_e as small as possible. Of these three factors, the most important is the antenna capacitance. Since a cylindrical dipole has a much larger capacitance than a spherical double probe, the noise level of a cylindrical dipole can be made substantially lower than a spherical double probe, often by as much as 20 to 40 dB. Of the remaining two factors, R_S and ν_e, both can be minimized by making the area of the antenna as small as possible. For a cylindrical dipole, this means making the radius as small as possible. Unfortunately, this condition is not consistent with the condition for maintaining ideal voltmeter operation in the resistive coupling regime, so a compromise must be made between these two competing requirements. For a spherical double probe, the area cannot be reduced without significantly reducing the capacitance, which is a critical factor in maintaining ideal voltmeter operation in the capacitive coupling regime.

In closing the discussion of electric antenna noise levels, we note that the above model does not address the noise level near the electron plasma frequency and the electron cyclotron frequency. The impedance of the antenna has resonances near these frequencies that strongly affect the noise level. The analysis is beyond the scope of this review. For a detailed discussion of these resonance effects, see *Meyer-Vernet* [1979], *Kellogg* [1981], *Sentman* [1982], and *Meyer-Vernet and Perche* [1989].

MAGNETIC ANTENNAS

Two types of magnetic antennas are commonly used for wave magnetic field measurements: loops and search coils. Schematic diagrams of each are shown in Figures 11 and 12. In both cases the basic principle of operation is Faraday's law, which states that in a circuit of N turns a voltage

$$V = N \frac{d\Phi_m}{dt} \qquad (16)$$

is induced whenever the magnetic flux $\Phi_m = \int \vec{B} \cdot d\vec{A}$ through that circuit changes. The main difference between a loop and a search coil is that a search coil uses a high permeability core to concentrate the magnetic flux through the circuit, whereas a loop does not. For the dimensions normally employed for a magnetic antenna, 1 meter or less, the plasma has no effect on the response of the antenna. Also, short wavelength effects are usually not important.

For a properly designed antenna system, the noise level is controlled by the first element in the system, which for a magnetic antenna is the resistance noise of the wire in the sensing circuit. This simple consideration has important consequences for the design of a magnetic antenna. Since a loop is simpler, we start by discussing a loop antenna. Because mass is usually a critical factor, the antenna must be designed to make optimum use of the available mass. For a loop of circumference ℓ_c, the resistance is given by $R = \ell_c N/(\sigma s)$, where N is the number of turns, σ is the conductivity, and s is the cross-sectional area of the wire. The corresponding mass of the loop is given by $m = s\ell_c N\rho$, where ρ is the mass density of the material. If the area of the loop is A, it is easy to show using the above equations and Equation 16 (rewritten as $V = NA\omega B$), that the magnetic field noise level is given by

$$\frac{B_N^2}{\Delta f} = \left(\frac{\rho}{\sigma}\right)\left(\frac{\ell_c}{A}\right)^2 \frac{4\kappa T}{m\omega^2} \quad . \qquad (17)$$

The above equation shows that the noise level is independent of the number of turns. As the number of turns increases the signal voltage increases, but the resistance also increases, which increases the noise power ($V_R^2/\Delta f = 4\kappa TR$) in direct proportion to the signal power. If the total mass of the loop is fixed, the above equation also shows that the lowest noise level is achieved by choosing a material with the smallest possible ratio of mass density to conductivity, ρ/σ, and a shape that has the largest possible ratio of area to circumference, A/ℓ_c. Of the materials that usually can be used, aluminum is best, although copper and silver are only slightly inferior. A circular loop provides the best ratio of area to circumference. For a search coil similar considerations also apply, except that one must take into account the weight of the high-permeability core and the more complicated geometry of the winding around the core. Because of the large number of variables involved, a simple analytical solution does not exist for the optimum distribution of mass between the winding and the core. For most successful search coil designs the mass is divided about equally between the winding and the core.

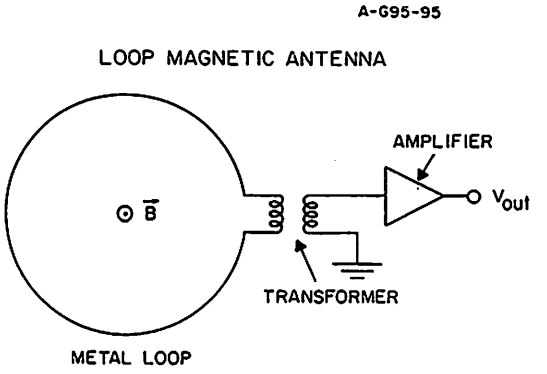

Figure 11. A sketch showing the principle of operation of a magnetic loop antenna. A loop antenna responds to the magnetic field component, B, perpendicular to the plane of the loop.

An important factor in the design of a magnetic antenna is the bandwidth. The bandwidth of a magnetic antenna is controlled by the inductance L and capacitance C of the sensing circuit and its associated electronics. A simple equivalent circuit that describes the frequency response of a magnetic antenna is shown in Figure 13. It is obvious from this simple circuit that a resonance exists at a frequency given by $\omega_{LC} = 1/\sqrt{LC}$. The resistor R_D is used to damp this resonance. Since the output voltage decreases very rapidly above the resonance frequency, ω_{LC} effectively determines the upper frequency limit of the antenna. To maximize the bandwidth, it is obvious that both the inductance and capacitance must be made as small as possible. First, we consider the inductance. Since the inductance varies as N^2, the number of turns must be made

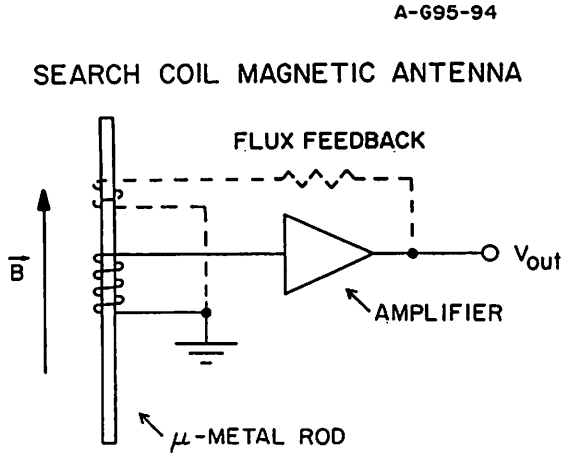

Figure 12. A sketch showing the principle of operation of a search coil magnetic antenna. A search coil responds to the component of the magnetic field, B, parallel to the axis of the μ-metal rod. Flux feedback is sometimes used to maintain a flat frequency response.

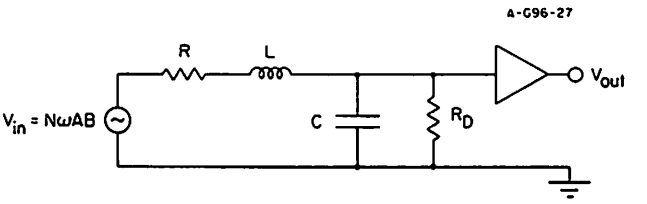

Figure 13. The equivalent circuit of a magnetic antenna. The quantities R, L, and C are the equivalent resistance, inductance and capacitance of the antenna. The resistor R_D is used to damp the resonant response of the antenna.

as small as possible. For a loop antenna, the minimum inductance is achieved by choosing N = 1 (i.e., one turn). Since the resistance of a one-turn loop of typical size and mass (1 meter diameter and 1 kg) is only a few milliohms, this optimization leads to a resistance noise that is much lower than the noise level of a typical transistor preamplifier. To assure that the resistance noise is above the noise level of the preamplifier, a transformer must be included between the loop and the preamplifier (see Figure 11). A typical turn ratio for this transformer is about 1:500. One of the penalties of using a loop is that the transformer introduces a low-frequency cutoff. The cutoff frequency is controlled by the mass and permeability of the transformer core [*Skilling*, 1959]. For a transformer of reasonable weight and size, the low-frequency cutoff is typically about 50 Hz.

For a search coil, the usual approach is to avoid the use of a transformer. This has the advantage of extending the frequency response down to much lower frequencies, the only limitation being the basic $d\Phi_m/dt$ response of the coil. The disadvantage is that to assure that the resistance noise of the wire is above the noise level of the preamplifier, a large number of turns must be used, which reduces the bandwidth. As the number of turns is increased, the cross-sectional area of the wire must be decreased (in order to maintain a fixed mass), which increases the resistance, hence increasing the resistance noise. Eventually a point is reached where the resistance noise of the wire exceeds the noise level of the preamplifier. This condition determines the minimum number of turns, N_{min}, hence the inductance of the coil. Since the upper cutoff frequency, $\omega_{LC} = 1/\sqrt{LC}$, is controlled by the inductance, the noise level of the preamplifier plays a crucial role in determining the bandwidth. To maximize the bandwidth, it is critical that the noise level of the preamplifier be made as low as possible.

Next we consider the capacitance. For a loop, the capacitance is determined mainly by the secondary winding on the transformer. For a search coil, the capacitance is determined mainly by the capacitance of the coil.

Minimizing these capacitances is a complicated process. However, procedures do exist that lead to near optimum solutions. For a discussion of the techniques involved, see *Welsby* [1960]. Once the capacitance has been determined, the frequency response of the antenna (not including the low-frequency cutoff of the transformer) can be represented rather accurately by the equation $V_{out} = \omega G(\omega) B A_{eff}$, where $G(\omega)$ is a normalized frequency response given by

$$G(\omega) = \frac{1}{\sqrt{\left(1 + \frac{R}{R_D} - \omega^2 L^2 C^2\right)^2 + \left(\frac{\omega L}{R_D} + \omega RC\right)^2}} \quad . \tag{18}$$

and A_{eff} is an effective area that takes into account the geometry of the antenna. Typical plots of the normalized frequency response for a loop and a search coil are shown in Figure 14. For comparable sizes and sensitivities the upper cutoff frequency of a loop antenna is usually considerably higher than the upper cutoff frequency of a search coil. However, as discussed earlier, the loop has a low-frequency cutoff that does not exist for a search coil.

For a loop, the effective area is simply the area of the loop, $A_{eff} = A$. For a search coil, the effective area depends on several factors, the most important of which are the geometry and permeability of the core. Although the core is usually made of rectangular layers of μ-metal (to reduce eddy current losses), for modelling purposes it is usually assumed that the core consists of a long thin ellipsoid of revolution. If the core has a relative permeability μ, it can be shown [*Bozorth*, 1951] that the effective permeability, $\mu_{eff} = B_{inside}/B$, of an ellipsoidal core is given to a good approximation by the equation

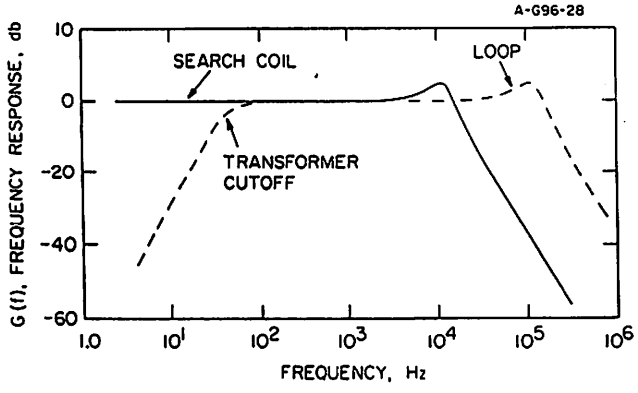

Figure 14. A comparison of the normalized frequency response, G(f), of a loop and a search coil. Loop antennas usually have higher upper frequency cutoffs than search coils. However, loop antennas have a low-frequency cutoff due to the transformer.

$$\frac{1}{\mu_{eff}} = \frac{1}{\mu} + \left(\frac{2a}{L}\right)^2 [\ell n(L/a) - 1] \quad , \tag{19}$$

where a is the radius at the center of the core and L is the tip-to-tip length of the core. Since the permeability μ is dependent on temperature and various other factors, it is desirable that the first term on the right-hand side of the above equation be small compared to the second term, i.e., $\mu > (L/2a)^2$. Since the largest μ values that can be achieved are about 10^5, this condition places an upper limit on the length to diameter ratio of the core ($L/a \lesssim 100$). If the above condition is satisfied, the effective permeability of the core is then given to a good approximation by the equation

$$\mu_{eff} = \frac{(L/2a)^2}{\ell n(L/a) - 1} \quad . \tag{20}$$

Since the cross-sectional area at the center of the core is πa^2, the effective area then becomes

$$A_{eff} = \pi (L/2)^2 \frac{1}{\ell n(L/a) - 1} \quad . \tag{21}$$

The above equation shows that the effective area of a search coil is approximately $\pi(L/2)^2$, which is the same as the effective area of a loop with a diameter equal to the length of the core. In practice, the effective area differs somewhat from the above equation due to the finite size of the coil and deviations from an ellipsoidal geometry.

Before finishing the discussion of magnetic antennas, let us return again to the noise level. The earlier analysis of the noise level of a magnetic loop antenna, given by Equation 17, does not take into account the resonant response of the antenna. To correctly take into account the effect of the resonance on the noise level, the real part of the impedance, Z_r, must be computed looking back into the antenna from the terminals of the preamplifier (see Figure 13). The noise voltage spectral density at the terminals of the antenna is then given by $V_N^2/\Delta f = 4\kappa T\, Z_r$. Proceeding as before, but now computing the noise voltage from the real part of the impedance, it is easy to show that the noise level of a loop antenna is given by

$$\frac{B_N^2}{\Delta f} = \left(\frac{\rho}{\sigma}\right)\left(\frac{\ell_c}{A}\right)\frac{4\kappa T}{m\omega^2}\left[\frac{\left(1+\frac{R}{R_D}-\omega^2 LC\right)+\frac{\omega L}{R}\left(\frac{\omega L}{R_D}+\omega RC\right)}{\left(1+\frac{R}{R_D}-\omega^2 LC\right)^2+\left(\frac{\omega L}{R_D}+\omega RC\right)^2}\right] \quad . \tag{22}$$

A similar result can be derived for a search coil antenna. The term in the rectangular bracket is the ratio of the real part of the impedance to the resistance in the wire, Z_r/R. Usually, the damping resistance, R_D, is small compared to the resistance, R, so we can assume that $R_D < R$. At low frequencies it is easy to see that the term in brackets reduces to one, which simply corresponds to the fact that at low frequencies $Z_r = R$. In this limit, Equation 22 agrees with the earlier result given by Equation 17. Proceeding upward in frequency the first evidence of a deviation from $Z_r = R$ occurs at a transition frequency given by $\omega_{RL} = \sqrt{R R_D}/L$. Above this frequency the real part of the impedance increases as ω^2. This frequency dependence is illustrated in Figure 15, which shows a plot of Z_r/R as a function of ω. At even higher frequencies the real part of the impedance eventually reaches a peak at the resonance frequency, ω_{LC}, and then decreases rapidly with increasing frequency, varying asymptotically as $1/\omega^2$.

As can be seen from Figure 15, the noise level of a magnetic antenna is enhanced above the resistance noise of the wire over a wide range of frequencies. Although the enhanced noise level cannot be avoided, the frequency range over which it occurs can be minimized. The low-frequency limit of the enhanced noise level is controlled by the R-L transition frequency, $\omega_{RL} = \sqrt{R R_D}/L$. To minimize the frequency range over which the enhanced noise level occurs, ω_{RL} should be made as large as possible. This means that R_D should be made as large as possible. However, to minimize the peak in the frequency response, the damping resistance should be adjusted to give critical damping. Thus, a compromise must be made between achieving the lowest possible noise level and minimizing the resonant peak in the frequency response.

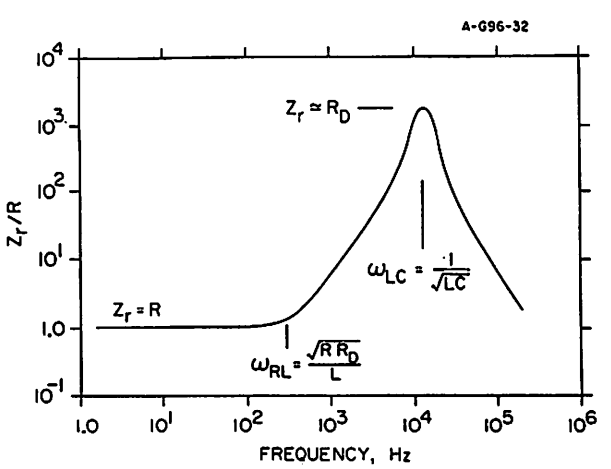

Figure 15. The ratio of the real part of the impedance, Z_r, of a magnetic antenna to the resistance, R, of the wire plotted as a function of frequency.

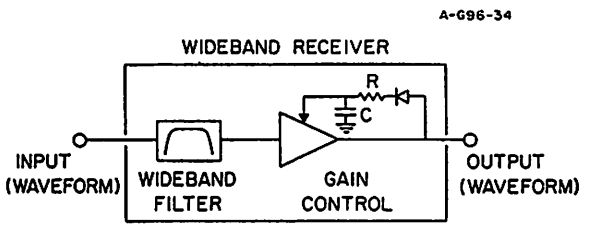

Figure 16. A block diagram of a wideband receiver. Since the entire waveform is transmitted to the ground, this type of receiver provides the highest possible resolution. An automatic gain control is used to reduce the dynamic range of the output waveform.

Usually the damping resistance can be made somewhat larger than the critical damping value without causing an unacceptable peak in the frequency response. For a search coil, flux feedback (see Figure 12) can also be used to control the resonant response of the antenna, thus avoiding the need for the damping resistor.

ON-BOARD SIGNAL PROCESSING

Space plasma waves measurements place great demands on signal processing. The ideal approach, of course, is to transmit waveforms from all the antennas directly to the ground where analyses can be performed with whatever frequency and time resolution are desired. However, one can easily show that for the bandwidths and dynamic ranges involved (1 to 10 MHz and 120 dB) the data rates are much too large. Therefore, a substantial amount of processing must be performed on board the spacecraft. There are two types of on-board processing, analog and digital. Since the techniques involved are quite different, these two types of processing are discussed separately.

Analog Processing

In the early days of space plasma wave research, all on-board signal processing was carried out via analog electronics. Although many different types of analog processing systems have been used, they can be categorized into three main types: (1) wideband receivers, (2) multi-channel spectrum analyzers, and (3) sweep frequency receivers. A block diagram of a wideband receiver is shown in Figure 16. As the name implies, this type of receiver simply transmits all of the signals within a relatively wide range of frequencies. Usually, an automatic gain control is employed to reduce the dynamic range of the signals that must be transmitted to the ground. A block diagram of a multi-channel spectrum analyzer is shown in

Figure 17. This type of spectrum analyzer consists of a bank of continuously active narrowband filters, each followed by an amplifier and some type of diode rectifier or root-mean-square detector. The detector output is usually averaged using a simple RC circuit to provide an output proportional to the average signal strength. A block diagram of a sweep frequency receiver is shown in Figure 18. This type of receiver consists of a single channel that is electronically swept in frequency via a circuit called a frequency converter. A frequency converter uses a nonlinear device to generate a frequency $f_1 = f_0 \pm f$, where f is the frequency of the input signal and f_0 is the frequency of a variable frequency oscillator. By using a fixed-frequency filter at f_1, the frequency of the input signal can be selected by adjusting the frequency of the oscillator. In modern designs, the oscillator is replaced by a frequency synthesizer. A frequency synthesizer generates a frequency that is a fixed integer fraction, M/N, of some basic reference frequency, usually derived from a crystal oscillator.

Each of the above types of receivers has inherent advantages and disadvantages. Wideband receivers come closest to the ideal by transmitting the entire waveform to the ground for analysis. However, wideband receivers inherently involve very high information rates, typically hundreds of kbits/sec. Since such a high information rate usually cannot be provided continuously over long periods of time, wideband receivers are best suited for relatively short bursts of data in regions of special interest. Multi-channel analyzers have inherently good time resolution since each channel is continuously active. However, each channel requires a separate filter and associated electronics, so the required weight and power increase linearly with the number of channels. Although miniaturization and low-power electronics have minimized these limitations, it is seldom possible to afford more than a few tens of channels.

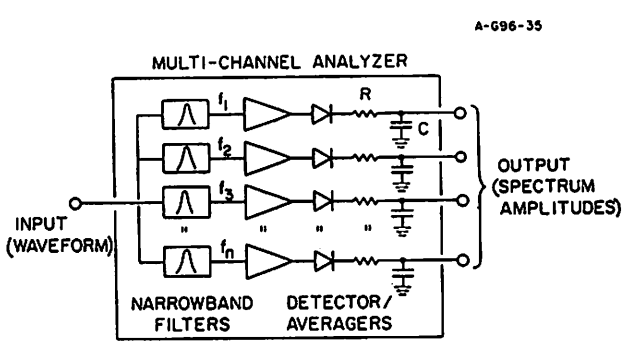

Figure 17. A block diagram of a multi-channel spectrum analyzer. Since each channel is continuously active, this type of receiver provides very good time resolution, but relatively poor frequency resolution.

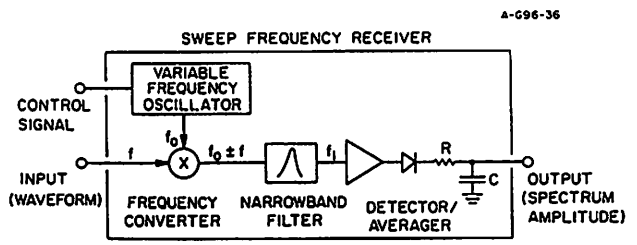

Figure 18. A block diagram of a sweep frequency receiver. Since the frequency is continuously variable, this type of receiver provides very good frequency resolution, but relatively poor time resolution.

Thus, although the time resolution of a multi-channel analyzer is very good, the frequency resolution is poor. Sweep frequency receivers suffer from essentially the opposite problem. Since the frequency is variable over an essentially continuous range, the frequency resolution is very good. However, since the receiver must dwell at each frequency for an interval at least equal to the filter response time, $\Delta t = 1/\Delta f$, the time that is required to sweep over the entire frequency range increases linearly with the number of frequency steps. Thus, although the frequency resolution is very good, the time resolution is poor.

Since each of the above receivers has its inherent advantages and disadvantages, an approach that has often been used is to include all three in the same instrument (see for example, *Gurnett et al.* [1995]). Thus, the wideband receiver provides very good frequency and time resolution for short periods of time, the multi-channel analyzer provides continuous spectrums with very good time resolution but relatively poor frequency resolution, and the sweep-frequency receiver provides continuous spectrums with very good frequency resolution but relatively poor time resolution.

Digital Processing

In recent years there has been a strong trend toward the use of on-board digital signal processing. For a plasma wave instrument digital signal processing offers several important advantages, including (1) much greater flexibility, (2) elimination of nonlinear distortion effects that are common in analog circuits, and (3) much smaller phase and amplitude errors.

The main difficulty with on-board digital signal processing is computational speed. Typical computations involve the use of Fourier transforms, digital filters and various types of auto- and cross-correlations. For a discussion of some of the algorithms involved, see *Cunningham* [1992]. Computations of this type are very demanding. For example, a Fourier transform using the

Cooley and Tukey [1965] method takes approximately N $\log_2$ N operations to compute a N-point transform. Thus, a 1024-point transform requires about 10^4 operations. To perform such computations in real time for a 1-MHz bandwidth and a dynamic range of 120 dB (20-bit resolution) requires approximately 10^7 20-bit operations per second. Such high computational rates are well beyond the reach of present space-qualified microprocessors. However, rapid advances are being made. A system that performs a 1024-point transform over a 22 kHz bandwidth with 12-bit resolution has already been flown [*Bougeret et al.*, 1995]. One can anticipate that in the not-too-distant future virtually all on-board plasma wave processing will be carried out using digital techniques.

CONCLUSION

In this chapter we have reviewed the principles of space plasma wave instrument design. Among the various topics considered, the most complicated involve electric antennas. Although the basic elements of electric antenna design are known, there are still parameter regimes that are poorly understood. For example, all current theories assume that the Debye length is much smaller than the tip-to-tip length of the antenna, $\lambda_D \ll L$. Although this condition is rarely violated for relatively long, 100 m antennas, significant uncertainties arise when shorter antennas are used, which are more likely to have $\lambda_D \gtrsim L$. Also, the response of an electric antenna to an externally applied electric field is still poorly understood in the vicinity of the electron plasma frequency and the electron cyclotron frequency.

Compared to electric antennas, the principles that affect the design of magnetic antennas are well known. Nevertheless, magnetic antennas suffer from several problems, the most important of which is low sensitivity. The basic sensitivity issue is almost entirely one of size and weight. Whereas electric antennas have typical dimensions of 100 m, for mechanical reasons magnetic antennas seldom have dimensions greater than 1 m. Since both types of antennas draw their energy from a volume of approximately L^3, where L is the characteristic size of the antenna, it is not surprising that for equal energy densities (i.e., E = cB), electric antennas have much better sensitivities than magnetic antennas. The most obvious approach to improving the sensitivity of a magnetic antenna is by cooling the antenna to low temperatures, possibly using super-conducting wires. Techniques of this type deserve further investigation.

The new era of on-board digital signal processing also poses significant challenges. Although the technical capabilities have not yet advanced to the point where the entire bandwidth of interest can be processed in real time, it is likely that such capabilities will some day exist. Since it is unlikely that communication rates will improve significantly, plasma wave investigators will be faced with difficult choices regarding exactly what type of information should be transmitted to the ground. One promising technique that may provide some relief is the rapidly evolving field of data compression. Recently, techniques have been demonstrated for transmitting frequency-time spectrums using compression factors of ten or more with little apparent degradation in the quality of the spectrums. Data compression techniques of this type are likely to play an increasingly important role in the processing of space plasma wave data.

Acknowledgments. The author thanks Ann Persoon, George Hospodarsky, Bill Schintler, and Don Kirchner for their assistance and comments during the preparation of this paper. This research was supported by NASA through contract 958779 with the Jet Propulsion Laboratory.

REFERENCES

Allcock, G., McK., A study of the audio-frequency phenomena known as "dawn chorus," *Australian J. Phys.*, *10*, 286-298, 1957.

Barkhausen, H., Zwei mit Hilfe der neuen Verstärker entdeckte Erscheinungen, *Phys. Z.*, *20*, 401-403, 1919.

Barrington, R. E., and J. S Belrose, Preliminary results from the very-low-frequency receiver aboard Canada's Alouette satellite, *Nature*, *198*, 651-656, 1963.

Bougeret, J.-L., et al., Waves: The radio and plasma wave investigation on the Wind Spacecraft, *Space Sci. Rev.*, *71*, 231-263, 1995.

Bozorth, R. M., *Ferromagnetism*, pp. 845-849, Van Nostrand, N. York, 1951.

Burton, E. T., and E. M. Boardman, Audio-frequency atmospherics, *Proc. IRE*, *21*, 1476-1494, 1933.

Cauffman, D. P., and D. A. Gurnett, Satellite measurements of high latitude electric fields, *Space Sci. Rev.*, *13*, 369-410, 1972.

Cooley, J. W., and J. W. Tukey, An algorithm for the machine computation of Complex Fourier Series, *Mathematics of Computation*, *19*, 297-301, 1965.

Cunningham, E. P., *Digital Filtering: An Introduction*, Houghton-Mifflin, Boston, 1992.

Dowden, R. L., Low frequency (100 kc/s) radio noise from the aurora, *Nature*, *184*, 803, 1959.

Duncan, R. A., and G. R. Ellis, Simultaneous occurrence of subvisual aurorae and radio noise on 4.6 kc/s, *Nature*, *183*, 1618-1619, 1959.

Eckersley, T. L., Musical atmospherics, *Nature*, *135*, 104-105, 1935.

Ellis, G. R., Low-frequency radio emission from aurorae, *J. Atmos, Terrestr. Phys.*, *10*, 302-306, 1957.

Fahleson, U. V., Theory of electric field measurements conducted in the magnetosphere with electric probes, *Space Sci. Rev.*, *7*, 238-262, 1967.

Feng, W., D. A. Gurnett, and I. H. Cairns, Interference patterns in the Spacelab 2 plasma wave data: Lower hybrid waves driven by pickup ions, *J. Geophys. Res.*, *98*, 21,571-21,580, 1993.

Fuselier, S. A., and D. A. Gurnett, Short wavelength ion waves upstream of the Earth's bow shock, *J. Geophys. Res.*, *89*, 91-103, 1984.

Gallet, R. M., The very-low-frequency emissions generated in the Earth's exosphere, *Pro. IRE*, *47*, 211-231, 1959.

Gurnett, D. A., and B. J. O'Brien, High-latitude geophysical studies with satellite Injun 3, 5, Very-low-frequency electromagnetic radiation, *J. Geophys. Res.*, *69*, 65-89, 1964.

Gurnett, D. A., et al., The Polar plasma wave instrument, *Space Sci. Rev.*, *71*, 597-622, 1995.

Hancock, J. C., *An Introduction to the Principles of Communication Theory*, p. 196, McGraw-Hill, N.Y., 1961.

Helliwell, R. A., Whistlers and related ionospheric phenomena, Stanford Univ. Press, Stanford, C.A., 1965.

Kelley, M. C., F. S. Mozer, and U. V. Fahleson, Measurements of the electric field component of waves in the auroral ionosphere, *Planet. Space Sci.*, *18*, 847-865, 1970.

Kellogg, P. J., Calculation and observation of thermal electrostatic noise in the solar wind, *Plasma Physics*, *23*, 735, 1981.

Jordan, E. C., *Electromagnetic Waves and Radiating Systems*, Prentice-Hall, Englewood Cliffs, N.J., 1950.

LaBelle, J., and P. M. Kintner, The measurement of wavelength in space plasmas, *Rev. Geophys.*, *27*, 495-518, 1989.

Langmuir, I., The interaction of electron and positive ion space charges in cathode sheaths, *Phys. Rev.*, *33*, 954-989, 1929.

Meyer-Vernet, N., On natural noises detected by antennas in plasmas, *J. Geophys. Res.*, *84*, 5373-5377, 1979.

Meyer-Vernet, N., and C. Perche, Tool kit for antennae and thermal noise near the plasma frequency, *J. Geophys. Res.*, *94*, 2405-2415, 1989.

Meyer-Vernet, N., et al., Measuring plasma parameters with thermal noise spectroscopy, this issue, 1997.

Mozer, F. S., Instrumentation for measuring electric fields in space, *Small Rocket Instrumentation Techniques*, pp. 26-34, North-Holland, Amsterdam, 1969.

Preece, W. H., Earth currents, *Nature*, *49* (1276), 554, 1894.

Scarf, F. L., G. M. Crook, and R. W. Fredricks, Preliminary report on detection of electrostatic ion waves in the magnetosphere, *J. Geophys. Res.*, *70*, 3045-3060, 1965.

Sentman, D. D., Thermal fluctuations and the diffuse electrostatic emissions, *J. Geophys. Res.*, *87*, 1455-1472, 1982.

Shawhan, S. D., Magnetospheric plasma waves, in *Solar System Plasma Physics, Vol. III*, edited by L. J. Lanzerotti, C. F. Kennel, and E. N. Parker, pp. 211-270, North-Holland, Amsterdam, 1979.

Skilling, H. H., *Electrical Engineering Circuits*, pp. 336-338, Wiley, N. York, 1959.

Stix, T. H., *The Theory of Plasma Waves*, McGraw-Hill, N.Y., 1962.

Storey, L. R. O., An investigation of whistling atmospherics, *Phil. Trans. Roy. Soc.*, London, A, *246*, 113-141, 1953.

Storey, L. R. O., Antennae electrique dipole pour reception TBF dans l'ionosphere, *L'onde Elec.*, *45*, 1427-1435, 1965.

Temerin, M., Doppler shift effects on double-probe measured electric field power spectra, *J. Geophys. Res.*, *84*, 5929-5934, 1979.

Warwick, J. W., J. B. Pearce, R. G. Peltzer, and A. C. Riddle, Planetary radio astronomy experiment for Voyager missions, *Space Sci. Rev.*, *21*, 309-327, 1977.

Welsby, V. G., *The Theory and Design of Inductance Coils*, pp. 144-151, MacDonald, London, 1960.

Donald A. Gurnett, Department of Physics and Astronomy, University of Iowa, Iowa City, IA 52242.